

**AN IMPROVED MODEL FOR TWO-DIMENSIONAL
TURBULENT BASE FLOW WITH ZERO MASS BLEED**

Summary Report

for

Contract NAS 8-11482

Marshall Space Flight Center

NATIONAL AERONAUTICS AND SPACE ADMINISTRATION

FACILITY FORM 602

N66 21439
(ACCESSION NUMBER)

36
(PAGES)

CR-71527
(NASA CR OR TMX OR AD NUMBER)

(THRU)

(CODE)

(CATEGORY)

By

J. P. LAMB

C.S. LENZO

Department of Mechanical Engineering

THE UNIVERSITY OF TEXAS

Austin

GPO PRICE \$ _____

CFSTI PRICE(S) \$ _____

Hard copy (HC) \$ 2.00


Microfiche (MF) \$ 1.50

February 28, 1966

I. INTRODUCTION

Of considerable importance in the design of rocket-powered vehicles is a thorough knowledge of the heating load to the base region of the vehicle. This heating is due both to radiation by the hot exhaust gas and convection by the flow adjacent to the base. The heating problem becomes especially acute in multi-nozzle configurations as the underexpanded exhaust plumes impinge with each other and with the flow external to the vehicle, creating thereby a complex field of interacting transport processes.

Some idea of this complexity may be gained by considering the region bounded by the rocket base, the nozzles, and the impinging jet plumes. Along the plume boundaries - the geometry of which are highly three-dimensional - there is a turbulent mixing and combustion process which involves simultaneous heat, mass, and momentum transfers between the hypersonic rocket exhaust, the base flow, and the external slipstream. To preserve continuity a portion of the gas along the plume inner boundaries must flow back toward the base of the vehicle. As this reverse flow strikes the baseplate, a stagnation point flow field is established. The base-plate flow is also three-dimensional, however, since the nozzles prevent a symmetrical venting of the rejected mass flux. The base thus receives heat both by boundary layer convection and by radiation from the hot plume surface through the intervening gas.



Some design data^{1*} have been obtained from experimental studies of the overall base heating process, but these have been hampered by the presently limited ability to accurately scale combustion phenomena. Much further experimental work on various details of the heating problem is necessary and some is presently underway. Very little progress, on the other hand has been made theoretically since one is faced with the interaction of many component processes, each of which represents a major effort of analysis.

Historically, supersonic wake investigations date back only about twenty years and, until recently, have been rather restrictive in their description of the base flow field. That is, most studies have characterized the wake region with a single pressure or a single temperature. This was permissible only because the secondary or base flow was a comparatively low speed flow and, in many instances, of minor importance. Such simplifications were included in the early Korst² theory, as well as the later analytical work on turbulent base flow of Nash³, Roberts⁴, and McDonald⁵.

In recent years, it has been recognized that secondary flows are indeed significant in some cases (notably in cavities⁶ and multi-nozzle bases⁷) and therefore theories such as those mentioned above have been unable to deal with these important physical problems. Thus, the present study was initiated in order to provide a more comprehensive theory for turbulent base flows which could

*Superscripts refer to references.

treat the multi-nozzle geometry.

As has been previously pointed out, the actual base heating problem is of such extreme complexity that direct analyses of the complete flow appear to have little chance of success. Consequently, the general approach of the present investigation was to begin with a comparatively simple two-dimensional geometry with isenergetic flow and then gradually introduce additional complications in order to bring the model closer to actual rocket base flow conditions.

Such a procedure is based on the hypothesis that one can devise a two-dimensional flow model whose dynamic and thermodynamic behavior is qualitatively the same as the actual multi-nozzle rocket. Some support for this approach comes from the theoretical analyses of Page et al⁸ as well as the experiments of Matz⁹. In addition, since one is attempting, through trial and error, to synthesize a complete treatment from various alternative component models, use of the comparatively simple two-dimensional geometry is attractive from the standpoint of simplicity since one can concentrate on the physical processes with a minimum of complication due solely to the geometry.

Although there is considerable experimental data (see Ref. 10 for a compilation) for two-dimensional backsteps without mass bleed, many investigators, as noted in the beginning, have reported the variation of only a single pressure in the base region. Thus

despite much study, many of the details of this, the simplest case of base flow, were still lacking prior to the work of Thomke¹¹, who presented extensive data on the wall pressure distribution throughout the entire backstep region as well as the location of the dividing streamline impingement. Even though these results were obtained with an axi-symmetric geometry, the step height was small compared to the body radius so that the base flow itself can be considered nearly two-dimensional.

It should also be noted that, while similar wall pressure distributions have also been reported by Hastings¹² for a two-dimensional geometry, the method of presentation of the results* precludes a direct comparison with theory. Furthermore, no measurements of the dividing streamline impingement were made. As will be subsequently observed, this latter information is extremely important in the development of the present base flow model.

Relying on such experimental guidance, the initial phase of the present investigation was therefore devoted to further exploration of this classical problem with the expectation that it would provide the necessary background for future work. The flow model which resulted from this portion of the study is discussed herein.

* Base pressures are referenced against a downstream pressure which cannot be easily calculated.

II. PRESENT THEORY

A. General Description

Although the major components* of the backstep flow field are well recognized, the aforementioned experimental studies of Thomke and Hastings have yielded an improved understanding of their interactions. For example, it has been found that the presence of an upstream boundary layer affects primarily the minimum value of base pressure and does not substantially alter the general shape of the wall pressure distribution in the recompression region. Such effects of boundary layers on minimum base pressure have been previously studied theoretically by Kirk¹³, Nash³, and McDonald⁵ with the rather simple "equivalent mass bleed" concept in conjunction with a hypothetical fully developed mixing zone. The same technique has been used in the present model and will be discussed in some detail later.

On the other hand, some of the more significant findings of these recent experimental investigations relate to the details of the impingement of the mixing layer with the wall. The data indicate that, at some distance above the wall, the shear layer interacts with the reverse flow which exists to preserve continuity. This point of interaction marks the commencement of recompression, downstream of which the static pressure is approximately equal to its value upstream of the step. Impingement of the dividing stream-

*The approach flow, Prandtl-Meyer expansion, free mixing layer, impingement and recompression zone, and redeveloping boundary layer.

line, which separates the primary flow from that recirculated to the base, occurs at a point about midway through the pressure rise.

The reverse flow generated at the impingement zone was considered to be of major importance since, with the multi-nozzle geometry, it is this flow which strikes the base plate and is vented between the nozzles. During the present study, therefore, special attention was devoted to the region downstream of the mixing zone-reverse flow interaction. In the following sections each component of the present model is examined in detail. By way of introduction, however, it is desirable to summarize the treatment (see Fig. 1).

As noted previously, the effect of an approach boundary layer is approximated by the method of Kirk which incorporates an asymptotic turbulent mixing theory. Utilizing an equivalent free jet for the reverse wall flow, a criterion is developed for calculation of the mixing zone termination or cutoff point. Downstream of this point the hypothetical inviscid flow is postulated to be an isentropic centered-wave (Prandtl-Meyer) compression in which the flow is turned to the local wall direction.

In calculating the inviscid boundary the continuous compression is replaced by a finite number of constant pressure steps which permits further application of the isobaric mixing theory and the integral continuity equation so that the locus of the dividing streamline, between the cutoff station and its impingement point at

the wall, can be determined. It is also shown that improved pressure distributions in the recompression region can be obtained with a comparatively simple correction based on the downstream boundary layer displacement thickness.

B. Expansion Zone and Mixing Layer

Although a detailed mathematical treatment of the expansion of a shear flow around a corner is available¹⁴, it is not convenient for engineering usage due to its complexity. On the other hand, the approximate method (for small δ) due to Nash³, considering isentropic expansion of each streamtube in the boundary layer, leads to a simple relationship between the initial (before expansion) and final (after expansion) values of the boundary layer momentum thickness.

$$\frac{\Theta_f}{\Theta_i} = \frac{(\rho_\infty U M_\infty^2)_i}{(\rho_\infty U M_\infty^2)_f}$$

which, in conjunction with the usual isentropic relations, and the ideal gas equation of state becomes

$$\frac{\Theta_f}{\Theta_i} = \left(\frac{p_i}{p_f} \right)^{\frac{k+1}{2k}} \left(\frac{M_{\infty i}}{M_{\infty f}} \right)^3 \quad (1)$$

In this expression p_f is the static pressure after the expansion and is equal to the base or cavity pressure, p_b . Thus, for specified approach conditions (Θ_i and $M_{\infty i}$) equation (1) determines

θ_f as a function of the Prandtl-Meyer turning angle. It should be noted that the inaccuracies introduced from this expansion model are largely compensated by the integral mixing theory.

In the approximate method of Kirk¹³ the final boundary layer momentum thickness is matched to that of a hypothetical mixing zone which begins at some virtual origin (point O in Fig. 2). The mixing layer coordinates (\tilde{x}, \tilde{y}) are thus referred to this point rather than the corner as in the case of no approach boundary layer. To determine the location of the virtual origin, expressions are required for the equivalent momentum thickness of the shear layer. Therefore, in the nomenclature of the Korst theory, one obtains

$$\begin{aligned}\theta_f &= \int_{-\infty}^{\tilde{y}_e} \frac{\rho u}{(\rho_0 v)_f} \left(1 - \frac{u}{v_f}\right) d\tilde{y} \\ &= (1 - C_{\infty f}^2) \frac{\tilde{x}_0}{\sigma} (I_{\eta_R} - I_{\eta_d}) = (1 - C_{\infty f}^2) \frac{\tilde{x}_0}{\sigma} I_{\eta_j}\end{aligned}\quad (2)$$

Also

$$\theta_f = \tilde{y}_j - \tilde{y}_d = \frac{\tilde{x}_0}{\sigma} [\eta_j - (\eta_d)_{\tilde{x}_0}] \quad (3)$$

where \tilde{x}_0 is the length of the imaginary portion of the mixing layer, σ is the spread or growth rate parameter, and $C_{\infty f}^2$ is the Crocco number of the inviscid flow after the Prandtl-Meyer expansion (analogous to $M_{\infty f}$). The subscripts j, d, and R in these equations refer respectively to:

1. The dividing streamline for zero mass bleed.

2. The dividing streamline for finite mass bleed.

3. The effective edge of the mixing layer, i.e., where $u \cong U$.

The combination of equations (1) and (2) yields an expression for \tilde{X}_o as a function of the Prandtl-Meyer angle α .

$$\tilde{X}_o = \Theta_i \left[\frac{\sigma}{(1-C_\infty^2) I_{ij}} \right]_{C_{\infty f}} \left(\frac{p_i}{p_f} \right)^{\frac{\gamma+1}{2\gamma}} \left(\frac{M_{\infty i}}{M_{\infty f}} \right)^3 \quad (4)$$

It is also observed from Fig. 2 that the perpendicular distance,

\tilde{Y}_o , from the inviscid jet boundary to the corner of the step is

$$\tilde{Y}_o = \Theta_f + \tilde{Y}_m - \tilde{Y}_j = \Theta_f + \frac{\tilde{X}_o}{\sigma} (\eta_m - \eta_j) \quad (5)$$

Furthermore, in terms of the primary space coordinates (x, y),

placed at the base of the step, one determines the location of the virtual origin as

$$\begin{aligned} X_o &= \tilde{Y}_o \sin \alpha - \tilde{X}_o \cos \alpha \\ Y_o &= h + \tilde{Y}_o \cos \alpha + \tilde{X}_o \sin \alpha \end{aligned} \quad (6)$$

where h is the step height. The combination of equations (1), (4),

(5) and (6) determines x_o and y_o for a particular expansion angle.

Now the mass flux which must be bled into the cavity to simulate the boundary layer is given by

$$\dot{m}_s = \int_{\tilde{Y}_o}^{\tilde{Y}_j} \rho u d\tilde{y} = \left[\rho u (1-C_\infty^2) \right]_f \frac{\tilde{X}_o}{\sigma} \left[I_{ij} - (I_{id}) \frac{\tilde{X}_o}{\sigma} \right] \quad (7)$$

where the value of $(\eta_d)_{\tilde{x}_c}$ is determined from equations (1), (3) and (4). The location of the dividing streamline at the cutoff point (where $\tilde{x} = \tilde{x}_1$) is determined from continuity considerations, i.e., the mass bleed due to the presence of the boundary layer is equivalent to the mass flux between the j and d streamlines at the cutoff point. Thus, from equation (7),

$$\tilde{x}_o [I_{1,j} - (I_{1,d})_{\tilde{x}_c}] = \tilde{x}_1 [I_{1,j} - (I_{1,d})_{\tilde{x}_1}]$$

or

$$(I_{1,d})_{\tilde{x}_1} = I_{1,j} - \frac{\tilde{x}_o}{\tilde{x}_1} [I_{1,j} - (I_{1,d})_{\tilde{x}_c}] \quad (8)$$

from which the value of $(\eta_d)_{\tilde{x}_1}$ can be found directly.

C. Mixing Zone Termination

At the beginning of the mixing layer-reverse wall flow interaction it is postulated that the velocity profile for the latter is equivalent to that of a jet which issues from a slot of infinitesimal width at some point downstream (see Fig. 3). Such a simplification of course violates the wall boundary condition although in the case of jet-to-jet impingement this would not be true since the wall becomes a plane of symmetry. The actual point of interaction or mixing zone cutoff is determined from two considerations:

1. The mass flux in the mixing layer below the dividing streamline must equal that in the reverse flow.

2. The outer edges ($u \approx 0$) of both the mixing and reverse flow profiles must coincide (point E of Fig. 3).

Now the mass flux above the wall in the reverse jet (of total width $2b$) is

$$\dot{m} = \int_0^b \rho u d\gamma = \rho_{\sim} u_{\sim} (1 - \zeta^2) b \tilde{I}_A \quad (9)$$

where $\rho_{\sim}, u_{\sim}, \zeta^2$ are reference quantities evaluated along the wall at the cutoff point. The integral \tilde{I}_A is analogous to the mass flux integral I_1 in the Korst mixing theory. That is

$$\tilde{I}_A = \int_0^1 \frac{\varphi}{1 - \zeta^2 \varphi^2} d\zeta$$

where

$$\zeta = \gamma/b$$

$$\varphi = u/u_{\sim} = 1 - \tanh^2 K \zeta$$

and K is a constant (taken as 3 in the present model). It will be recalled that hyperbolic tangent profile has been established for incompressible flow¹⁵. With such a universal profile \tilde{I}_A is solely a function of ζ^2 .

With isentropic relations and the ideal gas state equation, expression (9) can be written as

$$\dot{m} = \sqrt{\frac{K}{RT_0}} \tilde{M} \tilde{p}_0 \left(\frac{\tilde{p}}{\tilde{p}_0} \right)^{\frac{3k-1}{2k}} b \tilde{I}_A$$

(10)

Therefore in accordance with the previous continuity statement, the reverse mass flux is equivalent to the mixing layer mass flux below the dividing streamline, or

$$\tilde{p}_0 M_{0f} \left(\frac{\tilde{p}}{\tilde{p}_0} \right)^{\frac{3K-1}{2K}} \frac{\tilde{x}_1}{\sigma} (I_{1d})_{\tilde{x}_1} = \tilde{p}_0 M \left(\frac{\tilde{p}}{\tilde{p}_0} \right)^{\frac{3K-1}{2K}} b \frac{I_A}{\sigma} \quad (11)$$

From the geometry of Fig. 4 it is observed that

$$Y_0 = b + \tilde{y}_1 \cos \alpha + \tilde{x}_1 \sin \alpha \quad (12)$$

but the width of the mixing zone below the inviscid jet boundary is, in the Korst nomenclature,

$$\tilde{y}_1 = \frac{\tilde{x}_1}{\sigma} (\eta_m + 3)$$

Thus equation (12) become

$$b = Y_0 - \frac{\tilde{x}_1}{\sigma} [(\eta_m + 3) \cos \alpha + \sigma \sin \alpha] \quad (13)$$

The combination of equations (6), (11), and (13) yields, after rearrangement,

$$\frac{\tilde{x}_1}{\sigma} = \frac{h + \tilde{x}_0 \sin \alpha + \tilde{y}_0 \cos \alpha}{\frac{M_{0f}}{M} \frac{\tilde{p}_0}{\tilde{p}} \left(\frac{\tilde{p}}{\tilde{p}_0} \right)^{\frac{3K-1}{2K}} \left(\frac{\tilde{p}}{\tilde{p}_0} \right)^{\frac{1-3K}{2K}} \frac{(I_{1d})_{\tilde{x}_1}}{I_A} + (\eta_m + 3) \cos \alpha + \sigma \sin \alpha} \quad (14)$$

At the cutoff point no transverse pressure gradients are admitted so that the two static pressures appearing in the above equation are equal. This simplification, along with equations (3), (4), (5) and (8), permit equation (14) to be rewritten to

$$\frac{\tilde{x}_1}{\sigma} = \frac{h + \theta_i (1 - C_{\infty}^2)^{-1} (I_{1j})^{-1} \left(\frac{p_i}{p_e}\right)^{\frac{1-k}{2k}} (M_{oi}/M_{of})^3 I_a}{\frac{M_{of}}{M} \left(\frac{p_o}{p_e}\right)^{\frac{1-k}{2k}} \frac{I_{1j}}{I_A} + (\eta_m + 3) \cos \alpha + \sigma \sin \alpha}$$

(15)

where

$$I_Q = \sigma \sin \alpha + (\eta_m - \eta_d) \cos \alpha + \frac{M_{of}}{M} \left(\frac{p_o}{p_e}\right)^{\frac{1-k}{2k}} \frac{I_{1j} - (I_{1d})_{\tilde{x}_o}}{I_A}$$

which gives the cutoff distance as a function of α and p_o for given approach conditions.

D. Recompression Region

The theory of Korst as well as the Chapman model¹⁶ for laminar base flow employ an isentropic recompression criterion, viz., it is postulated that the dividing streamline possesses just sufficient mechanical energy to recompress to the static pressure downstream of reattachment. Thus all fluid below the dividing streamline ($u < u_d$) is recirculated to the base.

In recent years this recompression model has been the source of considerable misunderstanding among various investigators (for example, Nash³) who have interpreted the criterion very strictly: the dividing streamline must actually undergo an isentropic compression. Indeed, the resolution of this confusion was one of the primary motivations of the aforementioned study of Thomke.

On the other hand, the present analysis interprets the isentropic requirement in a very liberal sense: the dividing streamline is identified as the one which, at the cutoff point, could be isentropically compressed to the downstream static pressure. Further discussion of this significant feature will be subsequently presented.

The present model incorporates a centered-wave compression along the inviscid boundary between the cutoff point and the wall. The appropriate geometry is depicted schematically in Fig. 5. Considered as known quantities are the initial Prandtl-Meyer turning angle, α , and the coordinates (x_1, y_1) of the cutoff point as well as the Mach numbers before $(M_{\infty f})$ and after (M_w) the compression*. One must therefore determine first the location of the origin (x_c, y_c) of the fan and from this the coordinates (x_n, y_n) of any point on the boundary.

The wave origin is determined by recalling the relationship between radial lines in centered-wave (Prandtl-Meyer) flow¹⁷, viz,

$$\frac{r}{r^*} \sim \left(\frac{T_0}{T} \right)^{\frac{1}{2} \frac{k+1}{k-1}}$$

so that, in the present case,

$$\frac{r_1}{r_w} = \left[\left(\frac{T_0}{T} \right)_{M_{\infty f}} \left(\frac{T}{T_0} \right)_{M_w} \right]^{\frac{1}{2} \frac{k+1}{k-1}} \quad (16)$$

*Consequently the corresponding Mach angles ω_1 , and ω_w .

Now from the geometry one can write

$$r_1 = \frac{Y_c - Y_1}{\sin(\omega_1 - \alpha)} \quad (17)$$

and

$$r_w = \frac{Y_c}{\sin \omega_w} = Y_c M_w \quad (18)$$

which, together with equation (16), yield

$$Y_c = \frac{Y_1}{1 - M_w \sin(\omega_1 - \alpha)} \left[\left(\frac{T_0}{T} \right)_{M_{of}} \left(\frac{T}{T_0} \right)_{M_w} \right]^{\frac{1}{2} \frac{K+1}{K-1}} \quad (19)$$

Hence r_1 and r_w are known through equations (17) and (18).

Also from geometry

$$r_1 = \frac{x_c - x_1}{\cos(\omega_1 - \alpha)}$$

or

$$x_c = x_1 + r_1 \cos(\omega_1 - \alpha) \quad (20)$$

which, with equations (17) and (19), determines x_1 . The point (x_w) at which the inviscid boundary becomes tangent to the wall is found from the geometric relationship

$$r_w = \frac{x_c - x_w}{\cos \omega_w} = \frac{\sqrt{M_w^2 - 1}}{M_w} (x_c - x_w)$$

or

$$x_w = x_c - M_w (M_w^2 - 1)^{-1/2} r_w \quad (21)$$

This equation is used with equations (18) and (20) to find x_w .

For any arbitrary point on the boundary, relations analogous to equations (16), (17), and (20) can be written.

$$\frac{r_1}{r_n} = \left[\left(\frac{T_0}{T} \right)_{M_{\infty f}} \left(\frac{T}{T_0} \right)_{M_n} \right]^{\frac{1}{2} \frac{k+1}{k-1}} \quad (22)$$

$$r_n = \frac{y_c - y_n}{\sin(\omega_n - \nu_n)} \quad (23)$$

$$= \frac{x_c - x_n}{\cos(\omega_n - \nu_n)} \quad (24)$$

Inasmuch as any specified Mach number M_n (where $M_w < M_n < M_{\infty f}$) immediately determines the Mach angle (ω_n) and the change in turning angle ($\Delta \nu = \nu_{n-1} - \nu_n$) from standard relations, equations (22) and (23) may be solved for y_n and equations (22) and (24) for x_n .

Since it is desired to apply an isobaric mixing theory along the curved inviscid boundary, the continuous compression is approximated by a large number of constant pressure steps. Thus the quantities associated with M_n are assumed to be constant over a small length segment, the downstream end of which has coordinates x_n and y_n .

Shown schematically in Fig. 6 is such a segmented boundary with superimposed mixing layers. In each segment the usual relationship between transverse and longitudinal distances is assumed. That

is

$$\eta = \sigma \gamma / x$$

where η is the usual homogeneous space coordinate. Recalling that the Korst theory utilizes dual coordinate systems (physical and intrinsic) which are parallel but separated vertically by a distance y_m , one can write for the transverse distance d_q from the inviscid boundary

$$d_q = (\gamma - \gamma_m)_{Mq} = \left[\frac{\Delta S (\eta - \eta_m)}{\sigma} \right]_q \quad (25)$$

Since the angular difference between any two segments is small a second expression for d_q is obtained in terms of M_{n+1}

$$d_q = \left[\frac{\bar{S} (\eta - \eta_m)}{\sigma} \right]_{q+1} \quad (26)$$

Thus equations (25) and (26) can be solved for s_{q+1} , the virtual origin for the $(q+1)$ th segment, to give

$$\bar{S}_{q+1} = \left[\frac{\Delta S (\eta - \eta_m)}{\sigma} \right]_q \left[\frac{\sigma}{(\eta - \eta_m)} \right]_{q+1} \quad (27)$$

For the second interface one can write relations similar to (25)

and (26) for d_{q+1}

$$d_{q+1} = \left[\frac{\Delta S + \bar{S}}{\sigma} (\eta - \eta_m) \right]_{q+1} = \left[\frac{\bar{S} (\eta - \eta_m)}{\sigma} \right]_{q+2}$$

or

$$\bar{S}_{q+2} = \left[\frac{\Delta S + \bar{S}}{\sigma} (\eta - \eta_m) \right]_{q+1} \left[\frac{\sigma}{\eta - \eta_m} \right]_{q+2} \quad (28)$$

The combination of equations (27) and (28) thus yields

$$d_{j+1} = \left[\frac{\Delta S (\eta - \eta_m)}{\sigma} \right]_{j+1} + \left[\frac{\Delta S (\eta - \eta_m)}{\sigma} \right]_j$$

In the same manner one obtains

$$d_{j+2} = \left[\frac{\Delta S (\eta - \eta_m)}{\sigma} \right]_{j+2} + \left[\frac{\Delta S (\eta - \eta_m)}{\sigma} \right]_{j+1} + \left[\frac{\Delta S (\eta - \eta_m)}{\sigma} \right]_j$$

or in general

$$d_n = \sum_{j=1}^n \left[\frac{\Delta S (\eta - \eta_m)}{\sigma} \right]_j$$

Therefore the perpendicular distance between the inviscid boundary and the dividing streamline at any point ($s_n = \sum_{j=1}^n \Delta S_j$) along the curved boundary is given by

$$(Y_d)_n = \sum_{j=1}^n \left[\frac{\Delta S (\eta_d - \eta_m)}{\sigma} \right]_j \quad (29)$$

Thus the coordinates of the dividing streamline (X_d, Y_d) are (Fig. 7)

$$\begin{aligned} (X_d)_n &= x_n - (Y_d)_n \sin \nu_n \\ (Y_d)_n &= y_n - (Y_d)_n \cos \nu_n \end{aligned} \quad (30)$$

Where x_n , y_n , and ν_n are, respectively, the coordinates and turning angle of the inviscid boundary [see equations (22), (23), and (24)].

The value of η_d in equation (28) must be found from the integral continuity equation. A relation equivalent to equation (7) can be written for each pair of adjacent interfaces to give

$$\begin{aligned}\dot{m}_{q+1} &= p_0 \sqrt{\frac{K}{RT_0}} \left[M \left(\frac{p}{p_0} \right)^{\frac{3K-1}{2K}} \frac{\Delta S + \bar{S}}{\sigma} (I_{ij} - I_{id}) \right]_{q+1} \\ &= p_0 \sqrt{\frac{K}{RT_0}} \left[M \left(\frac{p}{p_0} \right)^{\frac{3K-1}{2K}} \frac{\Delta S + \bar{S}}{\sigma} (I_{ij} - I_{id}) \right]_{q+2}\end{aligned}$$

or

$$(I_{ij} - I_{id})_{q+2} = (I_{ij} - I_{id})_{q+1} \frac{\left[M \left(\frac{p}{p_0} \right)^{\frac{3K-1}{2K}} \frac{\Delta S + \bar{S}}{\sigma} \right]_{q+1}}{\left[M \left(\frac{p}{p_0} \right)^{\frac{3K-1}{2K}} \frac{\Delta S + \bar{S}}{\sigma} \right]_{q+2}} \quad (31)$$

However, use of equation (28), with the edge of the mixing layer ($\eta_R = \text{constant}$) as a reference point, gives

$$\begin{aligned}\left(\frac{\Delta S + \bar{S}}{\sigma} \right)_{q+1} \left(\frac{\sigma}{\Delta S + \bar{S}} \right)_{q+2} &= \\ &= \frac{\left(\frac{\Delta S}{\sigma} \right)_{q+1} + \left(\frac{\Delta S + \bar{S}}{\sigma} \right)_q \frac{(\eta_R - \eta_m)_q}{(\eta_R - \eta_m)_{q+1}}}{\left(\frac{\Delta S}{\sigma} \right)_{q+2} + \left(\frac{\Delta S + \bar{S}}{\sigma} \right)_{q+1} \frac{(\eta_R - \eta_m)_{q+1}}{(\eta_R - \eta_m)_{q+2}}}\end{aligned} \quad (32)$$

Thus equations (31) and (32) determine I_{id} at any point ($q+2$) along the boundary from which the corresponding value of η_d is found directly. Equations (28) through (32) thus enable one to move from the cutoff point toward the wall and calculate the locus of the dividing streamline.

Since the dividing streamline is always below the inviscid boundary (which becomes tangent to the wall) the dividing streamline will eventually cross the wall (point D in Fig. 7). In the present model this point of intersection is taken as the dividing streamline impingement and the static pressure at this point is taken as the stagnation pressure at the wall (point F in Fig. 3) for the reverse jet. That is

$$(p_h)_{(y_d)_h=0} = \tilde{p}_0 \quad (33)$$

Thus the reverse jet Mach number \tilde{M} , which also appears in equation (15), is determined by the isentropic pressure relation

$$\frac{p_b}{\tilde{p}_0} = f(\tilde{M}) \quad (34)$$

where p_b ($=p_f$) is the static pressure downstream of the initial Prandtl-Meyer expansion. The model thus postulates that the stream-tube of fluid just below the dividing streamline accelerates along the wall toward the base, expanding isentropically from a stagnation pressure \tilde{p}_0 at impingement to the static pressure at the cutoff point (p_b or p_f).

E. Reattaching Shear Layer Displacement Thickness

In the subsequent presentation of results, use will be made of the displacement thickness of the reattaching shear layer as a means of improving the predicted pressure distribution in the recompression region. Although it is recognized that the combination of a centered-wave compression and the isobaric mixing

theory is highly approximate, it is also known that the wall shear stress is of only minor significance in the reattachment process. Thus it is reasonable to expect that the mass flux in that portion of the mixing layer above the wall approximates the mass flux in the actual reattaching flow. The equivalent displacement thickness for any isobaric segment of the inviscid boundary is then (see Fig. 7)

$$\begin{aligned}
 \delta_n^* &= \int_{Y_w}^{Y_R} \left[1 - \left(\frac{\rho u}{\rho_\infty U_\infty} \right) \right] dY \\
 &= \left(\frac{\bar{S} + \Delta S}{\sigma} \right)_n \left[\eta_R - \eta_w - (1 - C_\infty^2) (I_{1R} - I_{1w}) \right]_n \\
 &= \left(\frac{\bar{S} + \Delta S}{\sigma} \right)_n (J_R - J_w)_n
 \end{aligned} \tag{35}$$

where

$$J(\eta) = \eta - (1 - C_\infty^2) I_1(\eta)$$

Using relations similar to those of the preceding section one can write

$$(Y_d)_n = \left[\frac{\bar{S} + \Delta S}{\sigma} (\eta_d - \eta_m) \right]_n \tag{36}$$

where $(Y_d)_n$ is known through equation (28). Thus

$$\left(\frac{\bar{S} + \Delta S}{\sigma} \right)_n = \frac{(Y_d)_n}{(\eta_d - \eta_m)_n}$$

and equation (35) becomes

$$\delta_n^* = \left[\frac{Y_d}{\eta_d - \eta_m} (J_R - J_w) \right]_n \tag{37}$$

The lower limit of integration in equation (37) can be found by combining equation (36) with a similar relation for $(Y_w)_n$ to obtain

$$\frac{Y_d}{Y_w} = \frac{\eta_d - \eta_m}{\eta_w - \eta_m}$$

or

$$(\eta_w)_n = (\eta_m)_n + (\eta_d - \eta_m)_n (Y_d / Y_w)_n$$

but, from the geometry (Fig. 7), one can relate Y_w to the coordinates and turning angle of the inviscid boundary by

$$(Y_w)_n = -\gamma_n \sec \psi_n$$

Thus

$$(\eta_w)_n = (\eta_m)_n - (\eta_d - \eta_m)_n \left(\frac{\gamma \sec \psi}{Y_d} \right)_n$$

from which $(J_w)_n$ is found directly.

F. Summary of Calculation Procedure

The procedure outlined below has been utilized to calculate base flow fields with the present model. A FORTRAN 63 program written for the Control Data Corporation Type 1604 machine was developed for this purpose.

For specified approach conditions ($M_{\infty 1}$, θ_1 , and h):

1. Assume a Prandtl-Meyer expansion angle α .
2. Assume a cutoff distance \tilde{x}_1 .
3. Locate the dividing streamline at cutoff with equations (4) and (8).
4. Construct the centered-wave inviscid boundary between cutoff and wall. Follow the dividing streamline to the wall and determine p_0 using the methods given in section IID.
5. Determine an improved value of \tilde{x}_1 with equation (15).
6. Repeat steps 3 through 5 until the value of \tilde{x}_1 converges.
7. Determine the value of b from equation (11) and compare with the lower edge of the mixing layer (point E in Fig. 3).
8. Repeat steps 1 through 7 until the edges of the reverse jet and mixing layer coincide at the cutoff distance \tilde{x}_1 .
9. If an improved pressure distribution in the recompression region is desired, compute the value of δ^* , using the procedure of Section IIE, at the point where the inviscid boundary becomes tangent to the wall (point x_w in Fig. 5). At this point move the wall up by the distance δ^* and, using the final values of α and \tilde{x}_1 found in step 8, construct a new inviscid boundary and impingement point.

REFERENCES

1. Sargent, R.J., "Base Heating Scaling Criteria For a Four-Engine Rocket Cluster Operating at High Altitude," AIAA Paper No. 65-826 (1965).
2. Korst, H.H., "A Theory for Base Pressures in Transonic and Supersonic Flow," J. App. Mech., 23, 593-600 (1956).
3. Nash, J.F., "An Analysis of Two-Dimensional Turbulent Base Flow Including the Effect of the Approaching Boundary Layer," National Physical Laboratory, Aerodynamics Division, Report 1036 (1962).
4. Roberts, J.B., "On the Prediction of Base Pressure in Two-Dimensional Supersonic Turbulent Flow," National Gas Turbine Establishment, Report R-265 (1964).
5. McDonald, H., "An Analysis of Turbulent Base Pressure Problem in Supersonic Axi-Symmetric Flow," Aero. Quart., Vol. 16, (1965).
6. Korst, H.H. and W.L. Chow, "Non-Isoenergetic Turbulent Jet Mixing Between Two Compressible Streams at Constant Pressure," Univ. of Illinois, ME TN 393-2 (1965).
7. Goethert, B.H. and R.J. Matz, "Experimental Investigation of Base Flow Characteristics of Four-Nozzle Cluster Rocket Models," AGARD Specialists Meeting on "The Fluid Dynamic Aspects of Space Flight," Marseille, France, April 1964.
8. Page, R.H. and R.J. Dixon, "Base Heat Transfer in a Turbulent Separated Flow," Fifth International Symposium of Space Technology, Tokyo, 1963.
9. Matz, R.J., Unpublished tests at AEDC (RTF).
10. McDonald, H., "The Turbulent Supersonic Base Pressure Problem: A Comparison Between a Theory and Some Experimental Evidence," British Aircraft Corporation, Report Ae 194, April 1965.
11. Thomke, G.J., "Separation and Reattachment of Separated Turbulent Boundary Layers Behind Downstream Facing Steps and Over Cavities," Douglas Aircraft Company, Report SM-43062, March 1964.
12. Hastings, R.C., "Turbulent Flow Past Two-Dimensional Bases in Supersonic Streams," Aeronautical Research Council, R and M No. 3401 (1965).

13. Kirk, F.N., "An Approximate Theory of Base Pressure in Two-Dimensional Flow at Supersonic Speeds," Royal Aeronautical Establishment, Tech. Note Aero 2377 (1959).
14. Pai, S.I., "Two Dimensional Supersonic Shear Flow Around a Corner," Proceedings of the Second National Congress on Applied Mechanics, 1954.
15. Schlichting, H., "Boundary Layer Theory," Fourth Ed., McGraw-Hill Book Company, New York, p. 605-607 (1960).
16. Chapman, D.R., "An Analysis of Base Pressure at Supersonic Velocities and Comparison with Experiment," NACA TN 2137 (July 1950).
17. Shapiro, A.H., "The Dynamics and Thermodynamics of Compressible Fluid Flow," Ronald Press Company, New York, p. 477 (1953).

FIG. 1 SCHEMATIC OF BASE FLOW FIELD

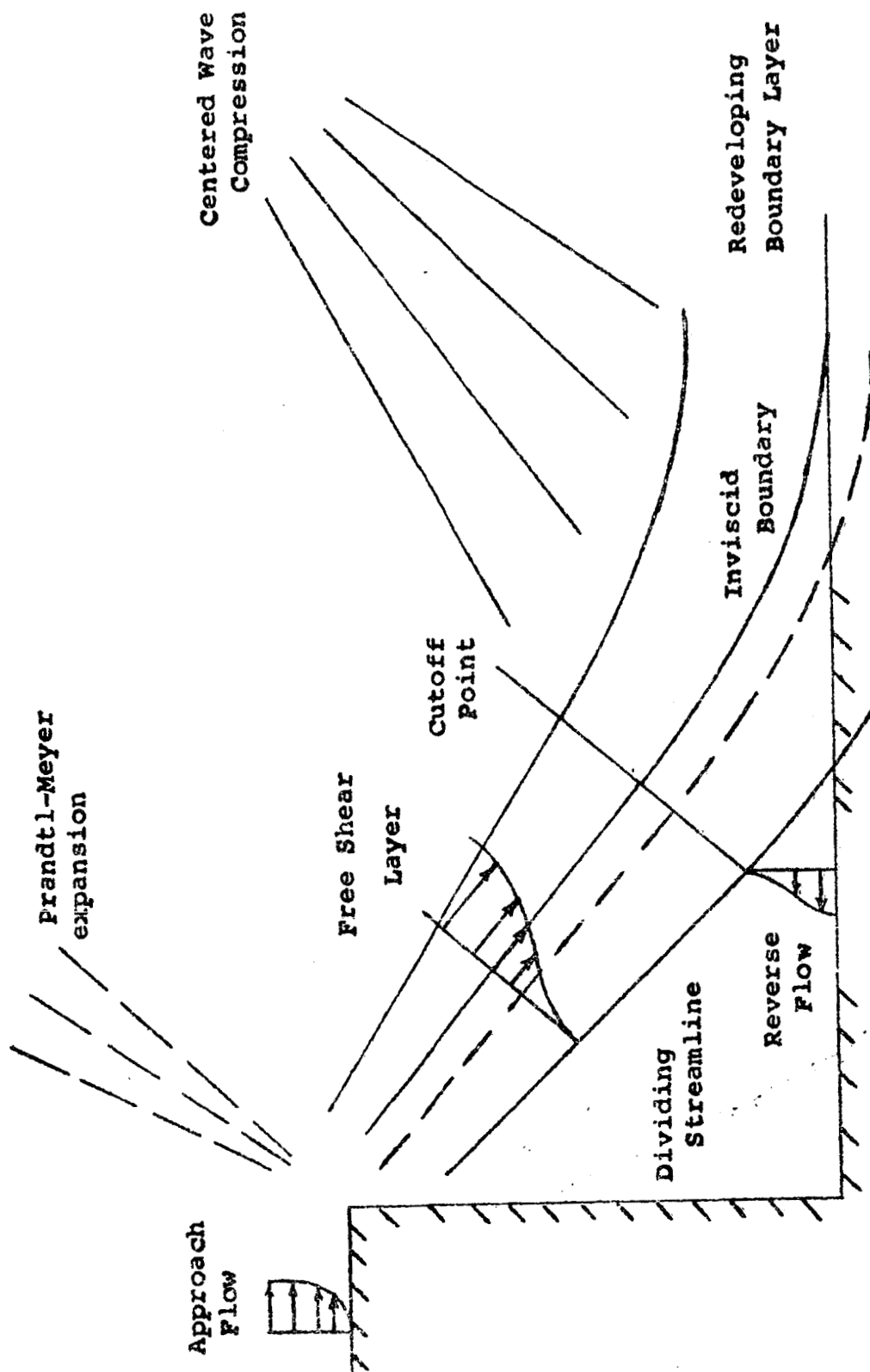


FIG. 2 SCHEMATIC OF VIRTUAL ORIGIN TECHNIQUE FOR
INITIAL BOUNDARY LAYER

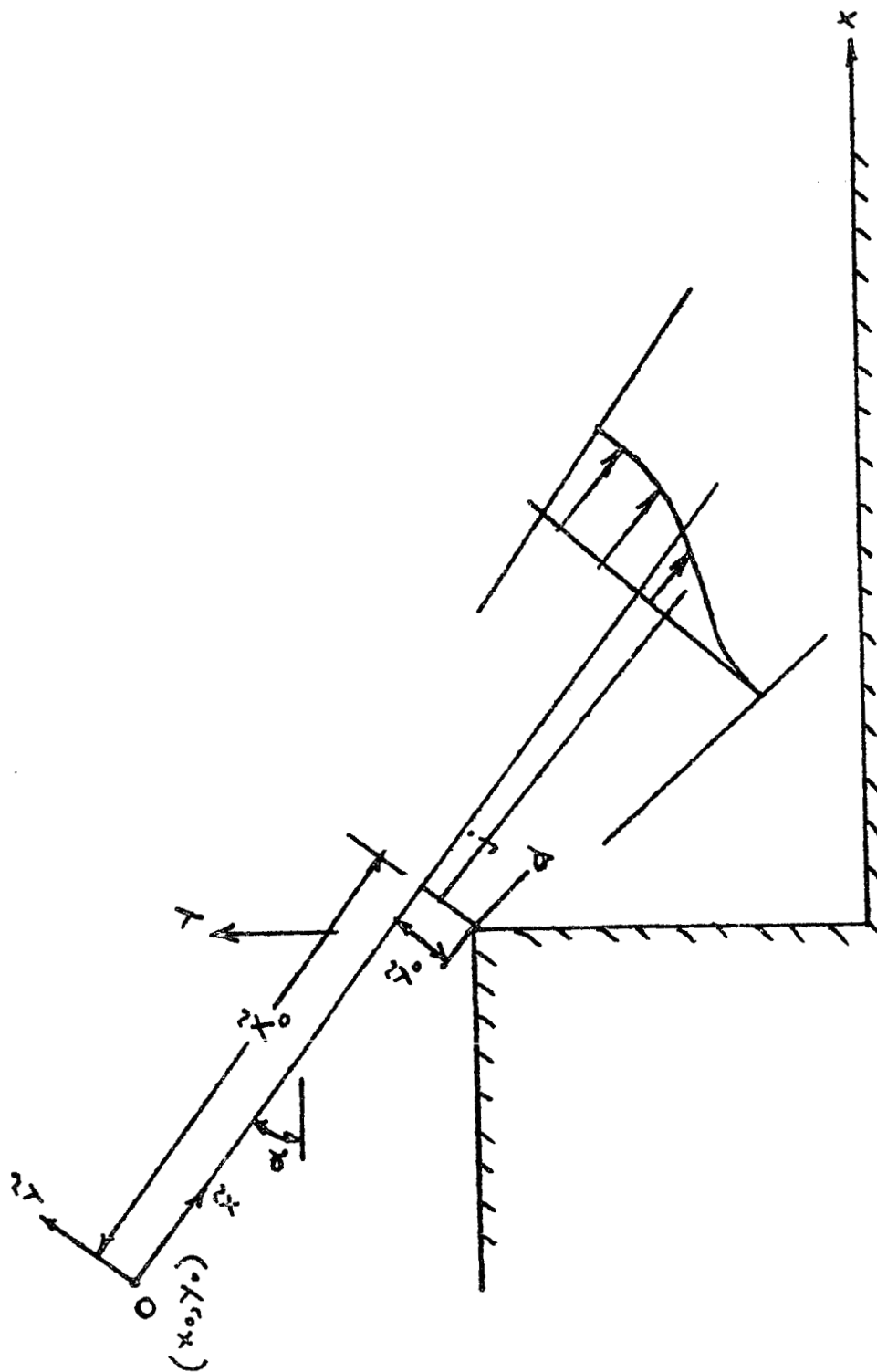


FIG. 3 DETERMINATION OF MIXING ZONE CUTOFF POINT

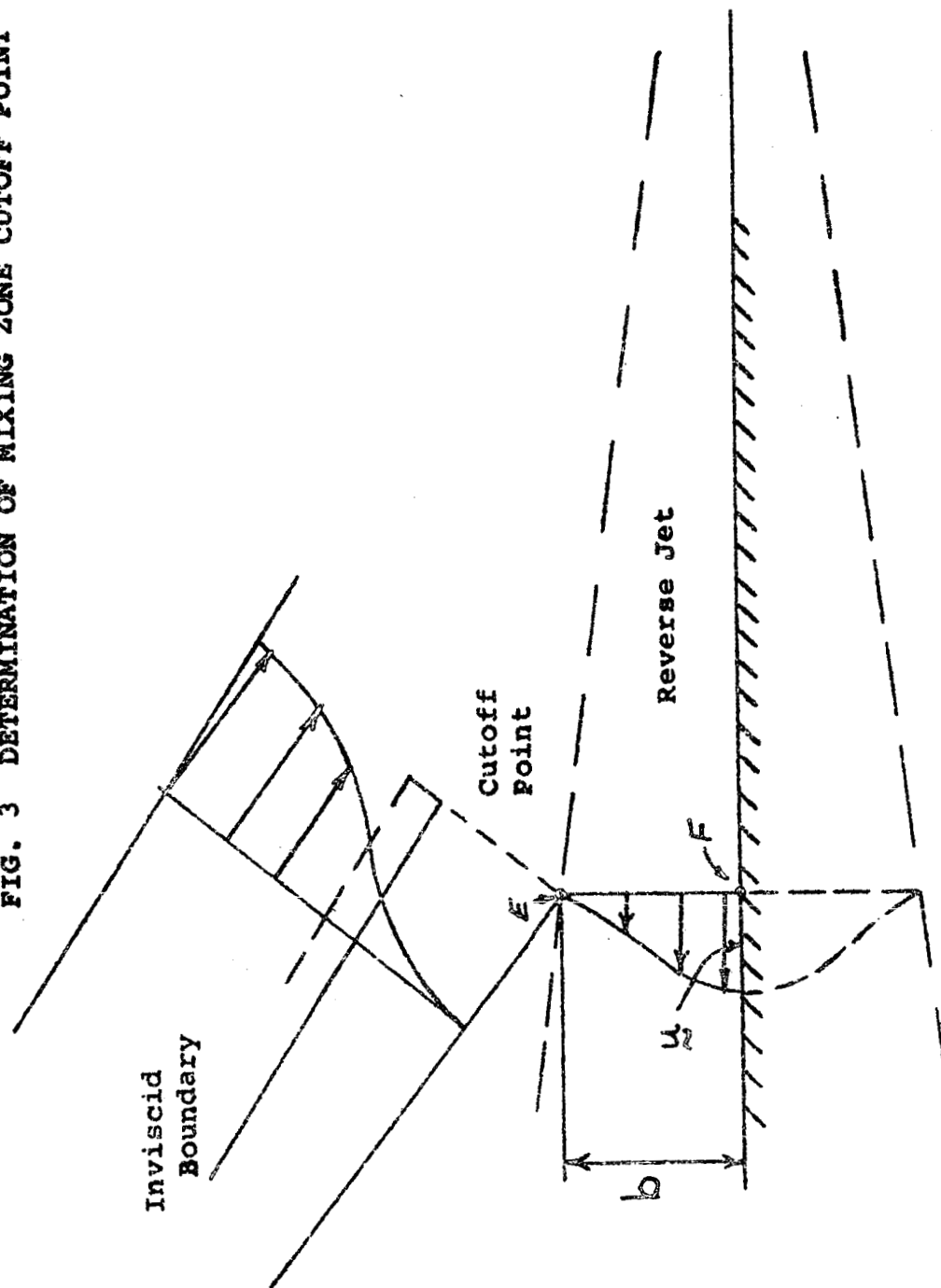


FIG. 4 GEOMETRY OF MIXING ZONE CUTOFF POINT

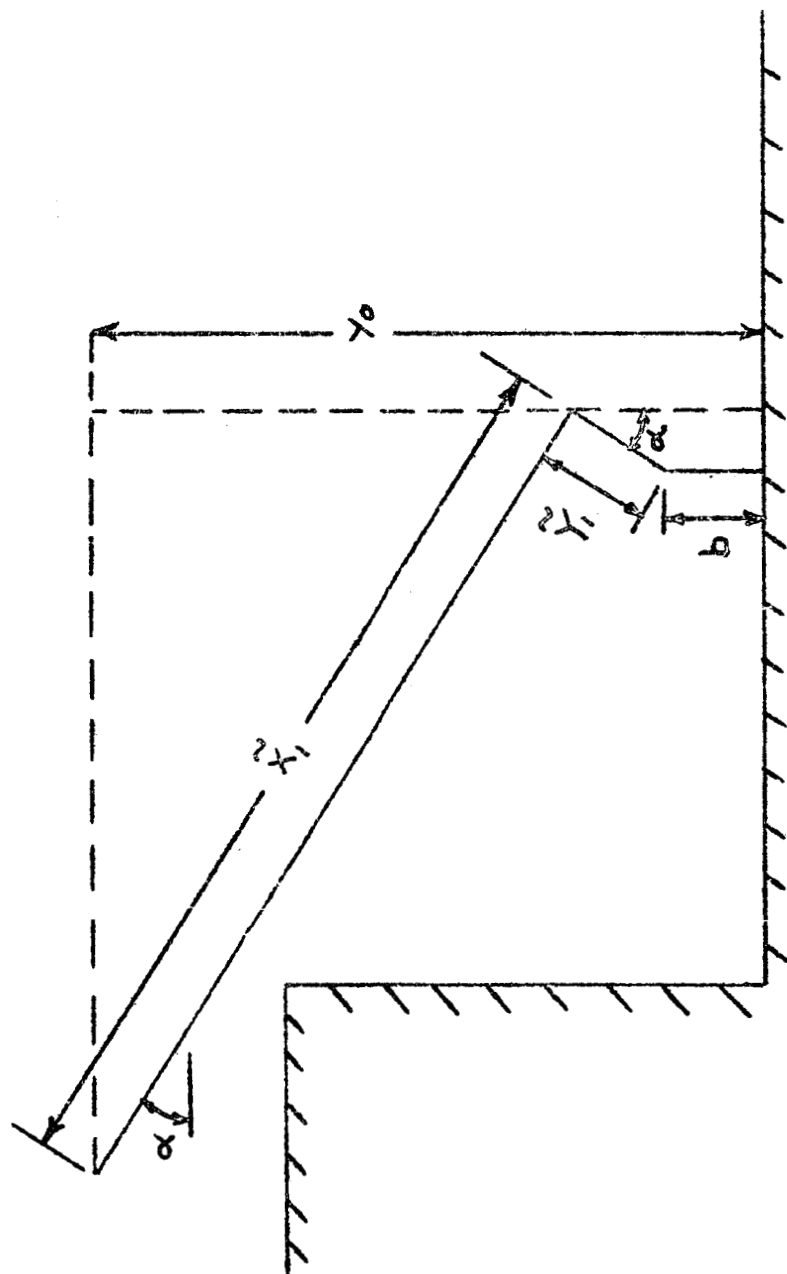


FIG. 5 SCHEMATIC OF CENTERED WAVE COMPRESSION ALONG INVISCID BOUNDARY

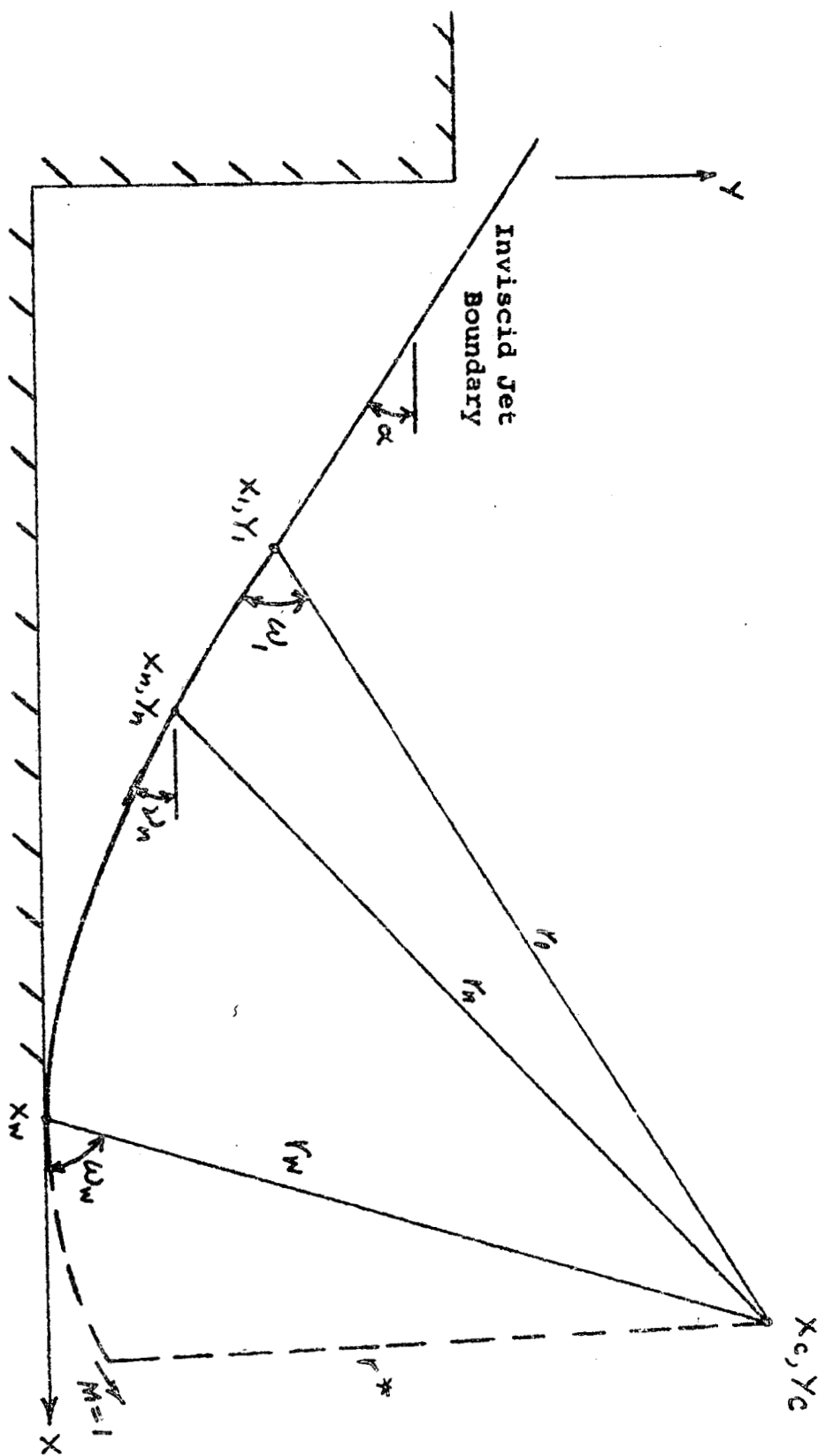
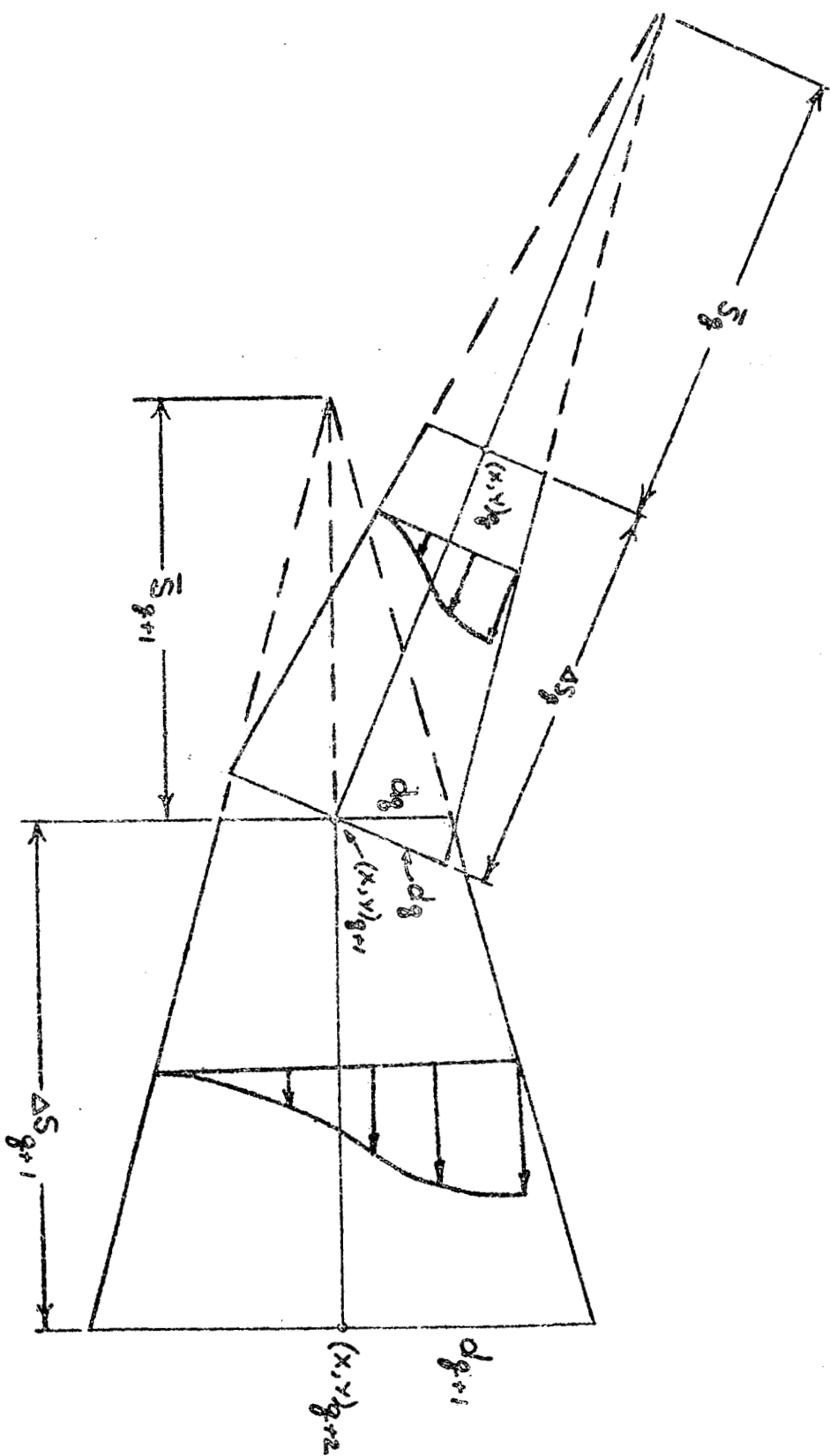


FIG. 6 APPLICATION OF ISOBARIC MIXING MODEL TO SEGMENTED
INVISCID BOUNDARY



The diagram illustrates a transonic flow field over a curved airfoil. The airfoil is on the left, with flow from left to right. A solid line represents the inviscid boundary, and a dashed line represents the viscous boundary. Key points and labels include: 'Cutoff Point' at the leading edge, 'Inviscid Boundary' label, 'Viscid Boundary' label, 'd' for distance, 'x_n, y_n' for a point on the boundary, '(x_d, y_d)_n' for a point on the dashed boundary, '(x_w)_n' for a point on the solid boundary, 'F' for a point on the airfoil, 'D' for a point on the dashed boundary, and 'p_n = p_0' for a pressure condition.

**Invlscid
Boundary**

(XIII)

$w(\rho \otimes \tau)$

 x, y, z

$(x_d, y_d)_n$

24

$$\angle p_1 = p_2$$

6